Editors' Suggestion

# Combination of ultrafast time-resolved spectroscopy techniques for the analysis of electron dynamics of heliumlike impurity centers in silicon

N. Dessmann,[1] S. G. Pavlov,[2] A. Pohl,[3] V. B. Shuman,[4] L. M. Portsel ⬮,[4] A. N. Lodygin ⬮,[4] Yu. A. Astrov ⬮,[4]
N. V. Abrosimov ⬮,[5] B. Redlich ⬮,[1] and H.-W. Hübers[2,3]

[1]*FELIX Laboratory, Institute for Molecules and Materials, Radboud University, 6525 ED Nijmegen, The Netherlands*
[2]*Institute of Optical Sensor Systems, German Aerospace Center, 12489 Berlin, Germany*
[3]*Institut für Physik, Humboldt-Universität zu Berlin, 12489 Berlin, Germany*
[4]*Ioffe Institute, Russian Academy of Sciences, 194021 St. Petersburg, Russia*
[5]*Leibniz-Institut für Kristallzüchtung (IKZ), 12489 Berlin, Germany*

We have combined ultrafast time-resolved techniques, available at European infrared free-electron laser facilities (HFML-FELIX and ELBE), for the analysis of intracenter relaxation processes in an atomiclike energy spectrum of the double donor magnesium in silicon. We show that complementary techniques enable the accurate analysis of complex transients inherent to strongly absorbing multilevel media. From the combined analysis of degenerate pump-probe, photon echo, and transient grating spectroscopy, we find short decay times of $(10 \pm 1)$ ps and $(30 \pm 3)$ ps for the $2p_0$ and $2p_{\pm}$ states, respectively. These high decay rates exceed those obtained earlier for the shallow, one-electron donors in silicon, where intracenter relaxation profits from interaction with a single phonon of a host lattice.

## I. INTRODUCTION

The investigation of recombination, relaxation, and coherence dynamics of impurities in semiconductors using time-resolved techniques at pulsed infrared free-electron lasers (FELs) has seen great interest in the past [1–3]. Most intensively studied over the last years are the group-V atoms in silicon (Si) and germanium (Ge) which are substitutional, single-electron donors and represent a hydrogen analog in the solid state, considered as promising candidates for building blocks in future quantum technology [4].

The incoherent population relaxation time ($T_1$) from excited orbital states to the impurity ground state can be derived from degenerate pump-probe spectroscopy [1,5] and decoherence times ($T_2$) can be measured by detecting photon echo decays [2]. Furthermore, high-quality crystal growth and precise doping of natural and isotopically enriched Si crystals by shallow donors as well as refined steady-state spectroscopy have led to high-quality spectral data. Near-lifetime-broadened (Lorentzian-shaped) absorption lines were shown [6–8] and appear to be in good agreement with the time-domain measurements [7]. In contrast to substitutional atoms in Si, magnesium (Mg, group-IIA) atoms are usually incorporated into the Si lattice by diffusion and occupy interstitial positions. They form double donor centers with a ground-state energy $E_i$ of ≈107 meV, which is about two times larger compared with shallow donors in Si. Hence the transition energies into the excited states are in the midinfrared region of the electromagnetic spectrum. From a practical point of view this opens up a platform for

optoelectronic applications in that spectral range, for instance, sensing in the midinfrared atmospheric windows [9].

It is assumed that phonon-mediated intracenter relaxation of excited states into the ground state dominates over all other processes, such as radiative and free-electron mediated relaxation. Therefore the correlation of impurity spectra to the spectra of lattice phonons and phonon combinations can have a large influence on the excited-state lifetimes. Mg has a binding energy between the shallow donors ($E_i$ between 42 and 71 meV) and the deeper, heliumlike group-VI donors in Si ($E_i$ between 199 and 318 meV). In the first case, single intervalley-phonon-assisted transitions (interaction energy below 60 meV) dominate intracenter relaxation. In the latter case, electron capture into the ground state can be assisted only by multiphonon interactions (overtones).

In a previous study we used the pump-probe (PP) technique to determine the relaxation times of the $2p_0$ and $2p_{\pm}$ states in Si:Mg [10]. Assuming a strong fast component in the PP response to be very likely a coherent artifact (CA), we analyzed a slow recovery component only. We then modeled the pump fluence-dependent signals with a rate equation approach and obtained a $T_1$ time of ≈270 ps for the $2p_0$ state and ≈530 ps for the $2p_{\pm}$ state. We concluded that there is a common bottleneck, which is determined by the last relaxation step between the lowest excited valley-orbit-split $1s(E)$ or/and $1s(T_2)$ state and the $Mg^0$ ground state. This last energy step is large, and therefore a one-phonon-assisted relaxation process is suppressed.

Since this study, important advances in understanding double donor physics and technology have been achieved,

which require revisiting this topic. In contrast to other impurity species, an isotopically enriched $^{28}$Si host lattice and the reduction of the donor density, responsible for isotopic and concentration line broadening, do not consequently reduce the spectral linewidth of $Mg^0$-related transitions [11]. The narrowest linewidth is $\approx 100$ $\mu$eV, which corresponds to a $T_1$ of only a few picoseconds in the lifetime-limited approximation. Furthermore, the binding energy of the para-valley-orbit-split states of neutral Mg donors was determined [12]. The energy gaps indicate that the $2p_0$ state can exhibit a fast decay due to the resonance of the interstate energy to the energy of the folded transverse acoustic (f-TA) intervalley phonon. In addition, we found high relaxation rates (lifetimes of tens to hundreds of picoseconds) for (deep) boron acceptors in diamond [12], while absorption spectroscopy revealed lifetime-limited linewidths [13]. This suggests that ultrafast relaxation of intracenter excitation could occur also for the energy gaps exceeding the energy of principal phonons in a semiconductor, for instance, by a two-step phonon-assisted process [14]. The efficiency of these processes has likely been underestimated in earlier studies.

These new insights allowed us to revisit our previous time-resolved measurements. In order to constrain the potential instrumental bias, we compared PP data obtained from different FEL facilities, and we decided to utilize complementary time-resolved spectroscopy techniques. We apply the transient grating (TG) technique to measure impurity center dynamics and the relaxation time $T_1$, and we use the photon echo (PE) decay to determine the decoherence time $T_2$. We found that the complementary use of all techniques supports the short lifetimes of excited states, as predicted from the spectral linewidths in high-resolution spectroscopy.

## II. SAMPLES

High-purity Si crystals, grown and purified by the float zone technique, were doped by Mg using a high-temperature diffusion technique, further developed and described in recent studies [15–18]. Thin high-purity (99.999%) Mg layers were deposited on the two surfaces of a Si wafer. This wafer was then "sandwiched" between two other Si wafers, and the "sandwich" was heated at $1250\,^\circ$C in a sealed quartz ampoule in an argon atmosphere for 7.5 h. To suppress the decomposition of the solid-state phase of the interstitial Mg and thus obtain a high Mg density, the ampoule was cooled in a stream of nitrogen immediately after the diffusion. The outer Si wafers and an additional layer of roughly 50 $\mu$m of the inner wafer were ground off. The samples were wedged and optically polished on both sides. The doping concentration was determined by calibrated infrared absorption and Hall experiments [19] (Table I).

## III. INFRARED ABSORPTION SPECTROSCOPY

We performed Fourier transform infrared spectroscopy (FTIR) with a Bruker Vertex 80V spectrometer and a Janis ST-100-FTIR liquid-He flow cryostat at a cold finger temperature as low as 6 K, and with a spectral resolution of 31 $\mu$eV; see Ref. [20] for experimental details. The cryostat was equipped with wedged diamond windows to suppress standing waves.

TABLE I. Parameters of the Si:Mg samples fabricated for this study.

| Sample | Thickness (mm) | $n$ ($10^{15}$ cm$^{-3}$) | |
| --- | --- | --- | --- |
| | | $Mg^0$ | $Mg^*$ |
| 98-1 | 1.3 | 1.3 | 0.1 |
| 138-2 | 0.94 | 1.28 | 0.3 |

The samples were put onto a gold-coated, polished copper sample holder and held in place by a rubber-based flexible glue only on the corners, in order to minimize strain on the sample when cooling down to low temperatures. A temperature difference of the sample of up to 10 K compared with the cold finger can be expected due to limited thermal conductivity of the glue. Because of the large binding energy of the $Mg^0$ ($\approx 1240$ K) and the large energy separation from the even-parity valley-orbit excited states $1s(T_2)$ and $1s(E)$ ($\approx 660$ K) [12] the slight elevation of the Si:Mg temperature has a negligible effect on the populations of the donor ground and excited states [12].

The absorption spectrum of a Si:Mg sample (sample 138-2) at $\approx 15$ K shows all major transitions from the $1s(A_1)$ ground state into the excited states (Fig. 1) which are expected from natural Si ($^{\mathrm{nat}}$Si) as a host material [11]. All $Mg^0$ donor intracenter transitions overlap with strong infrared-active two-phonon bands of Si (Fig. 1).

Additionally, the strongest $Mg^0$ transitions into the $2p_0$, $2p_\pm$, and $3p_\pm$ excited states are subject to or at the onset of absorption saturation at the given sample thickness and doping concentration [20].

In order to perform peak fits to the resonances, we removed the rather flat background of the infrared-active two-phonon
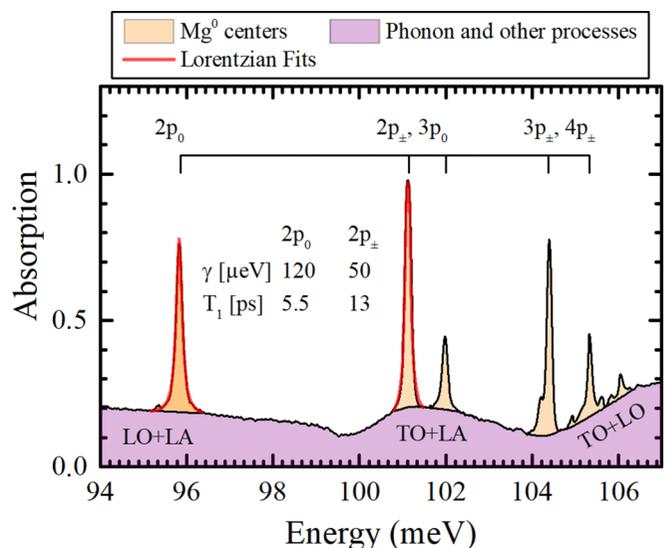


FIG. 1. FTIR absorption spectrum of a Si:Mg sample (sample 138-2) at $\approx 15$ K. For better distinction the resonant absorption lines are separated from the two-phonon background spectrum (purple) obtained for an undoped Si reference sample, The $2p_0$ and $2p_\pm$ lines are fitted with (saturated) Lorentz functions. LA, longitudinal acoustic; LO, longitudinal optical; TO, transverse optical.

bands (purple area in Fig. 1). We then fitted a Lorentzian peak function to the "background-free" data, taking the saturation of the absorption into account. It is known that inhomogeneous broadening effects cause a Gaussian distribution of the transition energies, transforming Lorentzian into Voigt line shapes. Our data analysis does not show any visible improvement of the line fits using a Voigt line shape instead of the Lorentzian fit. This indicates that the linewidth is dominated by homogeneous broadening, i.e., is lifetime limited. We obtain linewidths $\gamma$ of 120 and 50 $\mu$eV for the $1s(A_1)$ to $2p_0$ and $2p_\pm$, respectively. In a previous spectroscopic study conducted on Mg-doped $^{nat}$Si at temperatures down to the temperature of superfluid He (2.1 K), similar linewidths were observed [11]. The linewidths of $^{28}$Si:Mg are further reduced by approximately a factor of 2 as additional broadening due to the random isotopic Si distribution in the host lattice is reduced [11]. A lower limit of the $T_1$ lifetimes of the excited states can be derived indirectly from these data, as it is related to the inverse full width at half maximum (FWHM; $\gamma$) of the absorption lines [7,21]. We obtain a $T_1(2p_0)$ of 5.5 ps and a $T_1(2p_\pm)$ of 13 ps. Isotopic purification is believed to have only a small to vanishing effect on the actual dynamic lifetime [5,6].

## IV. TIME-RESOLVED EXPERIMENTS

We compare the time-resolved PP experiments performed with the free-electron laser FELBE (U100) at the Electron Linear Accelerator with High Brilliance and Low Emittance (ELBE) facility with Free-Electron Lasers for Infrared Experiments (FELIX) at the High Field Magnet Laboratory–FELIX (HFML-FELIX) facility. Both FELs emit near-bandwidth-limited pulses with a tunable wavelength and spectral width of typically below 0.5%, which correlates to a pulse duration of a few picoseconds. FELBE operates in a quasi-continuous-wave (quasi-cw) mode with a pulse repetition rate of 13 MHz. FELIX emits $\approx$10-$\mu$s-long macropulses at 10 Hz, where each macropulse contains micropulses at a fixed repetition rate. We used here a repetition rate of 25 MHz. All time-resolved techniques that we applied require the splitting of the incoming pulses with pellicle beamsplitters. The time of arrival at the sample is controlled by changing the optical paths with optical delay stages. The typical range of motion allows for a maximum time delay between pairs of pulses of $\approx$1 ns.

At the ELBE facility we applied PP spectroscopy, and at the HFML-FELIX facility we additionally implemented PE as well as TG spectroscopy into a single setup. In all cases the incoming beams are focused onto the sample and collimated after the sample by off-axis parabolic mirrors (OAPs). The incoming beams are positioned on the focusing OAP so that the angle between the wave vectors is on the order of 5° [Fig. 2(b)]. In the PP scheme, $k_1$ and $k_2$ denote the probe and pump beam, respectively. In the PE experiment, $k_1$ is the pump beam and $k_2$ is the rephasing beam. In the TG experiment, $k_2$ and $k_3$ are the pump beams that form the grating. After the sample, beams are either transmitted or created due to nonlinear interactions in defined (phase matching) directions $k_E$ (PE) or $k_G$ (TG) [Figs. 2(b) and 2(c)]. For any specific measurement we allow only one beam to pass to the detector,
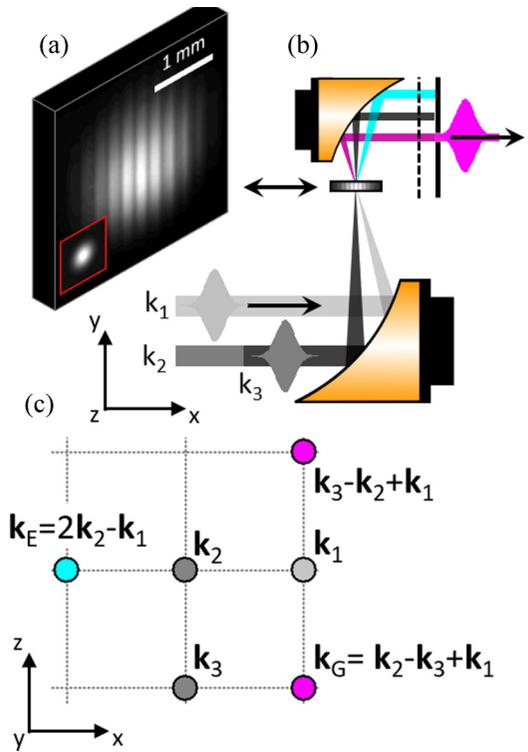


FIG. 2. (a) Intensity distribution of the FEL pulses with FELBE (at lower left, interpolated) and FELIX (at center, as measured) imaged with a pyroelectric focal plane array. The interference pattern in the center is caused by a second pump beam of same size and intensity arriving at an angle of $\approx$5°. (b) Schematic of the beam propagation near the sample. (c) Illustration of the beam directions on a plane after collimation. $k_E$ indicates the direction of the photon echo, and $k_G$ is the direction of the transient grating signal.

selected by an aperture on a motorized $x$-$y$ scanner. The stray light suppression is on the order of $10^5$.

The samples were mounted in a liquid-He flow cryostat as described above, and similarly cooled down to $\approx$15 K. The focus size at the sample position was measured with a pyroelectric camera and varies with the optical layout of the individual experimental setup. At ELBE the intensity FWHM was typically about 200–400 $\mu$m; at HFML-FELIX we chose to focus the light down to 1–2 mm [Fig. 2(a)]. The absolute pulse energy was measured with calibrated sensors (FELIX, SLT PEM 34 IR; FELBE, coherent PM-3) in front of the cryostat with an accuracy of $\approx$2%. We use these numbers to calculate the pulse energy per unit area. The intensity can be controlled by sets of infrared step attenuators (LASNIX).

### A. Degenerate pump-probe spectroscopy

With degenerate PP spectroscopy we measure the pump-induced change in the absorption coefficient of an optical transition with sufficiently weak, noncollinear pump and probe pulses (Fig. 2) at different times after the excitation. It is assumed to be an instantaneous event at $t = 0$, and the PP transient can be written in the form of a modulated transmis-

sion at the pump-probe photon energy:

$$\frac{\Delta T(t)}{T} = \frac{e^{\Delta\alpha(t)} - e^{\alpha}}{e^{\alpha}}, \quad (1)$$

with $\Delta\alpha = \alpha - \alpha(t) = \sigma d(N - N_e(t))$, where in our case $N$ is the equilibrium concentration of Mg donors in the ground state, $N_e(t)$ is the pump-induced change in the ground-state population after a time delay $t$, $d$ is the thickness of the sample, and $\sigma$ is the absorption cross section of a Mg center at the PP photon energy. If the relaxation process can be considered as a single-step decay (e.g., in a two-level medium or when dominated by one specific relaxation step), then

$$\frac{dN_e}{dt} = -\frac{1}{T_1}N_e(t). \quad (2)$$

$T_1$ is the lifetime of the probed excited state and describes the recovery of the ground-state population. In the case of small signal modulation and weak absorption, the measured PP signal is directly proportional to the population difference:

$$N_e(t) \propto -\ln\left(1 + \frac{\Delta T(t)}{T}\right) \approx \frac{\Delta T(t)}{T} = \frac{\Delta T(0)}{T}e^{-t/T_1}. \quad (3)$$

It is a common procedure in a PP experiment to repeat scans after successively reducing the pump laser fluence to the minimal detectable modulation of the transmission. If there is only one dominating decay constant at the lowest pump fluences, that time constant is identified with $T_1$. However, PP measurements often suffer from either too weak modulation or too strong (nonlinear) light absorption. Additionally, since most of the real electronic systems are inherently multilevel ones, extra levels (additionally pumped and/or probed) can contribute to the PP signal. It is possible but challenging to quantify these contributions by solving the balance equations of a multilevel system, while the accuracy decreases significantly with an increasing number of levels involved in the analysis. Especially when the signal does not recover to zero within the maximum applicable delay, the uncertainty becomes large.

In resonance with an electronic transition, coherent interactions between the probe and pump beam are enhanced. The most prominent example of such an interaction is the appearance of a coherent artifact when the polarizations of the beams are equal. The origin of this coherent artifact is the diffraction of the beams by an interference grating they produce, causing a periodic modulation of the excitation of the resonant absorption in the sample [22], similar to the transient grating method (see below). Also induced multiphoton absorption can contribute to a further complication of the signal shape and analysis [23].

In our previous PP study of the dynamics of the $2p_0$ and $2p_\pm$ relaxation at ELBE we observed several components in the PP signal. When the FEL is tuned exactly or close to a Si:Mg resonance, a short (several to several tenths of picoseconds) and a long (several hundreds of picoseconds) positive component (bleaching) appear (Fig. 3). In addition, the signal could drop below zero (induced absorption) around zero delay but recovers within a few picoseconds (Fig. 3, bottom). This effect depends strongly on the laser parameters such as pulse duration, i.e., spectral width, and detuning from resonance. It is more pronounced for the $2p_\pm$ state.
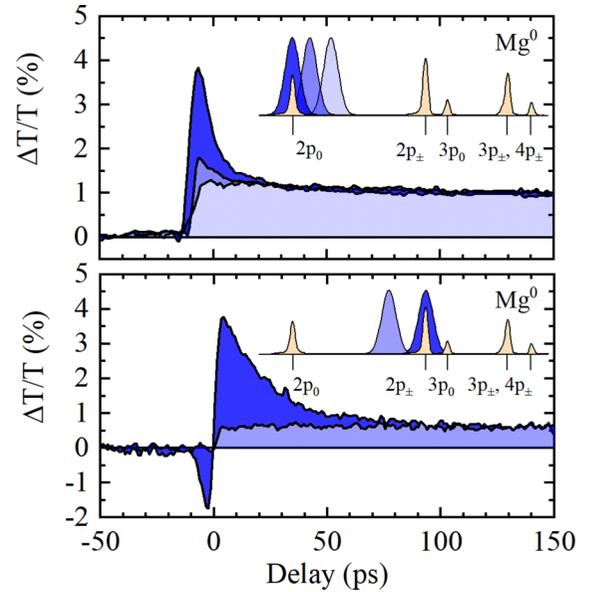


FIG. 3. Pump-probe signals for the $Mg^0$ $1s(A_1) \rightarrow 2p_0$ (top) and $2p_\pm$ (bottom) transitions (Si:Mg sample 98-1) in and out of resonance measured with FELBE. The signals consist of two components recovering on different timescales. The short component vanishes when tuning the FEL out of resonance. The FEL pump spectrum (blue) and Si:Mg absorption spectrum (light brown) are shown in scale.

Previously, we concluded that both short signal components are artifacts. We analyzed the slow component in the off-resonance case (light blue curve in Fig. 3), assuming it stems from the absorption modulation on the tail of the transition, effectively suppressing signals, which appear at shorter timescales when the maximum power of the FEL is exactly on resonance (Fig. 3, dark blue curve). We then modeled the resulting transients with rate equations for a three- and four-level system. Finally, we concluded that there was a $T_1$ of $\approx270$ ps for the $2p_0$ state and $\approx530$ ps for the $2p_\pm$ state. As described above, we revisited our data due to the large discrepancy between these results and the later-available steady-state spectroscopic data of the improved samples which hinted at much faster decay rates.

We reanalyzed the available PP data obtained at ELBE for on-resonance pumping and found that the decay constant of the short component is independent of the intensity of the pump pulses in all measurements. The extension to the three-level model did not deliver better fitting accuracy, indicating a single nonradiative step dominating in the intracenter relaxation path(s). The overall maximum modulation $\Delta T_{max}/T$ was kept below 5% (Fig. 4). Additionally, the modulation amplitude below 2% appears to follow a linear dependence with pump intensity.

We repeated the PP measurements at HFML-FELIX and found very similar signal shapes and decay constants for both the $2p_0 \rightarrow 1s(A_1)$ and $2p_\pm \rightarrow 1s(A_1)$ transitions [see Figs. 5(c) and 6(c)]. The maximum modulation at similar intensities was higher due to a better match of the FEL spectral linewidth and the absorption linewidth during these measurements. We choose a larger modulation for the data analysis
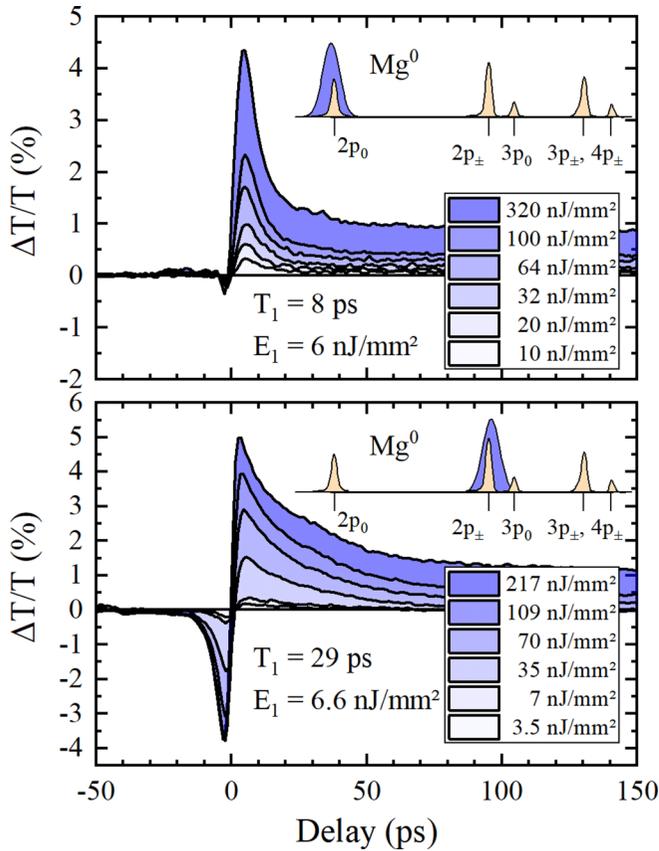
FIG. 4. Intensity-dependent pump-probe signals for the $Mg^0$ $1s(A_1) \to 2p_0$ (top) and $2p_\pm$ (bottom) (Si:Mg sample 98-1) transitions on resonance (see insets) measured with FELBE. The decay time of the short component remains unchanged with changing the laser intensity for both transitions. The FEL pump spectrum (blue) and Si:Mg absorption spectrum (light brown) are shown in scale.



FIG. 5. Comparison of photon echo (a), transient grating (b), and pump-probe (c) signals measured with FELIX when pumping resonantly (see inset) for the $Mg^0$ $1s(A_1) \to 2p_0$ transition (Si:Mg sample 138-2). The coherent artifact (CA) appears in the PP signal [(c), purple] when the pump and probe beams are parallel polarized. The FEL pump spectrum (red) and Si:Mg absorption spectrum (light brown) are shown in scale.

due to a reduced signal-to-noise ratio caused by the smaller duty cycle of FELIX compared with FELBE.

By recording PP traces with parallel and perpendicular polarizations of the beams, we were also able to discriminate the coherent artifact. It appears as an additive component to the transients with a short decay time. Both transients, perpendicular and parallel polarizations, converge to the same shape and amplitude after the coherent artifact has decayed. For the short negative component we suggest a photoinduced change in the energy spectrum, e.g., by the optical Stark effect. Nonetheless, a further systematic study is required. The component with the long time constant remains unchanged when tuning the FEL photon energy out of impurity resonance. The absence of any distinct power dependence of the amplitude of the differential absorption signal when tuning the laser away from resonance (Fig. 3) is one of the main problems with the original conclusions. It is likely that a second (slower) process is monitored independently and in parallel to the actual (fast) impurity-related electronic process. Since we see a rather flat two-phonon absorption background in the infrared absorption spectrum, the additional long decay times we observe in the PP signal could be caused by optically excited high-energy phonons. These phonons have anharmonic decay rates on the picosecond-to-nanosecond timescale and could form hot

spots [24] whose spatial and thermal transport is monitored by the PP technique. To confirm this, a comparative study with undoped Si samples would be helpful.

The time constants of the short components are in excellent agreement between the different facilities, $\approx$30 ps (FELIX) and $\approx$29 ps (FELBE) for the $2p_\pm$ state, and $\approx$10 ps (FELIX) and $\approx$8 ps (FELBE) for the $2p_0$ state. The scan-to-scan variation of these numbers is about $\approx$10% in all cases. Because of the lower duty cycle of FELIX compared with FELBE (quasi-cw) we expect a reduced influence of additional sample heating to the signal; we therefore believe that the FELIX decay times are closer to the low-temperature $T_1$ limit. In order to quantify this further, a temperature and duty-cycle-dependent PP study would be helpful. Overall, our time-resolved results are in much better agreement with the inverse spectroscopic absorption linewidths.

### B. Transient grating spectroscopy

The transient grating (TG) time-resolved technique is a special configuration of PP spectroscopy in which two coincident pump pulses interfere at the sample surface to generate a spatially periodic excitation profile with a characteristic grating period $\Lambda$ defined by the wavelength $\lambda$ and incident angle $\theta$ of the two pump pulses:

$$\Lambda = \lambda/(2\sin\theta). \tag{4}$$

This spatial periodicity (in our case, 50–100 $\mu$m) is encoded onto the modulation of material properties, from which a time-delayed probe beam can be diffracted to provide information about dynamics at a specific spatial length scale. The three-beam configuration implies that TG probes the medium
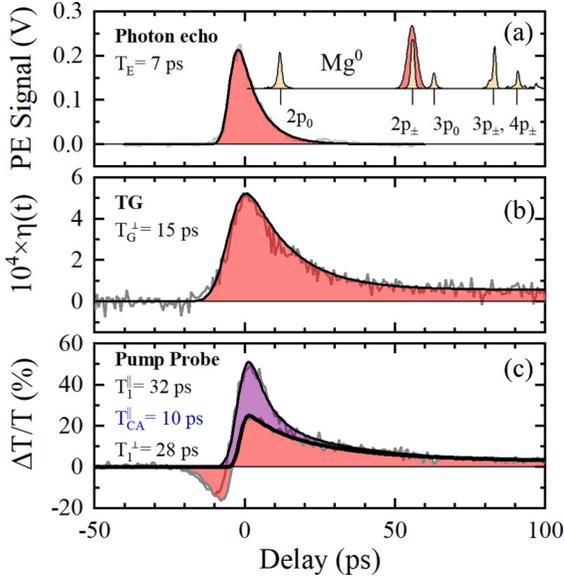
FIG. 6. Comparison of photon echo (a), transient grating (b), and PP (c) signals measured with FELIX when pumping resonantly (see inset) for the $Mg^0$ $1s(A_1) \rightarrow 2p_\pm$ transition (Si:Mg sample 138-2). The coherent artifact (CA) appears in the PP signal [(c), purple] when the pump and probe beams are parallel polarized. The FEL pump spectrum (red) and Si:Mg absorption spectrum (light brown) are shown in scale.

more precisely in space, i.e., in depth, which gives specific advantages against the PP technique for optically thick media. Another inherent advantage is the background-free nature of the experiment, which usually results in a higher signal-to-noise ratio than can be achieved with the modulation-based PP technique. The diffraction efficiency decays as

$$\eta_{\text{eff}}(t) = \eta_{\text{eff}}^0 \exp(-t/T_G). \tag{5}$$

We find typical grating efficiencies on the order of $10^{-3}$–$10^{-4}$ at rather low excitation fluences comparable to low-intensity PP measurements. This is detectable with very low background noise or allows us to reduce the excitation fluences even further. In general, the grating is modified not only by local relaxation but also by spatial propagation and diffusion phenomena [25] so that

$$\frac{1}{T_G} = \frac{2}{T_1} + \frac{8\pi^2 D}{\Lambda^2}, \tag{6}$$

where $D$ describes the diffusion decay of the grating. It is usually necessary to measure the TG signal at various grating periods, i.e., angles of incidence, and determine the value for $T_1$ through extrapolation. In our measurements we find $T_G$ values of $\approx 15$ and $\approx 6.5$ ps for the $2p_\pm$ and $2p_0$ states, respectively (Figs. 5 and 6). In comparison to the PP data, we see that $T_1 \approx 2T_G$. This indicates a grating decay dominated only by relaxation. This seems plausible since no physical mechanism transferring intracenter excitation from isolated impurity centers in space is presupposed and therefore one does not expect any additional diffusion decay. One major drawback of the TG method arises from the shorter signal decay and longer risetime, which can be problematic for short relaxation times approaching the pulse duration, as can be

seen in the $2p_0$ TG response data. We believe that the signal-to-noise ratio could be further enhanced compared with the present study by increasing the TG volume, e.g., using larger beam spots at the sample facet.

### C. Photon echo spectroscopy

When an ensemble of two-level oscillators is excited by a finite laser pulse, the individual oscillators initially radiate in phase and form a coherent polarization wave. The coherence loss over time is described with a characteristic time $T_2$, which can be divided as [7]

$$\frac{1}{T_2} = \frac{1}{2T_1} + \frac{1}{T_x}, \tag{7}$$

with $T_1$ being the relaxation time of the excited state and with additional losses of the coherence summarized in $T_x$. In the Bloch sphere scheme this is visualized by a linear superposition state created by the laser pulse [ideally on the equator of the Bloch sphere with a ("$\pi/2$") pulse] [2]. For each oscillator the superposition state precesses around the Bloch sphere. The total amplitude of the polarization decays due to the finite excited-state lifetime and the loss in coherence is caused by small variations in the local environment, causing the superposition states to fan out on the Bloch sphere. Both effects can be reversed and the initial coherence restored by a second ("$\pi$" or rephasing) laser pulse, which leads to the emission of the photon echo when all oscillators are oscillating in phase again. Experimentally, this is realized by noncollinear laser pulses so that the photon echo is geometrically separated from the other laser pulses, since it is emitted in the phase-matching direction and hence can be detected background-free [Fig. 2(c)].

For the case of vanishing other dephasing processes, $T_x \rightarrow \infty$, and $T_2$ is dominated by and can be used to determine the relaxation time $T_1$. In a multilevel system, however, phase loss will be defined by the characteristic time of the population loss out of the excited state. This includes not only "downward" motion in energy, when the relaxation into the ground state occurs through intermediate levels, but also "upward" motion by thermal excitation to neighboring, higher excited states. It is therefore possible, at least in principle and in a low-temperature limit, to discriminate between direct and multistep relaxation pathways. As shown in Ref. [2] experimentally, the intensity of the echo decays exponentially with an experimental decay time given by $T_E = T_2/4$. However, it was also shown that the PE decay is very sensitive to, and is shortened when increasing, the laser intensity and sample temperature [2].

We performed photon echo spectroscopy with FELIX. At the lowest temperatures and lowest intensities, resulting in a sufficient signal-to-noise ratio, we found dephasing times $T_2 = 4T_E$ of $\approx 28$ ps and $\approx 20$ ps for the $2p_\pm$ and $2p_0$ states, respectively [see Figs. 5(c) and 6(c)], and we can derive the respective $T_1$ values of $\approx 14$ ps ($2p_\pm$) and $\approx 10$ ps ($2p_0$). Both values support the short $T_1$ times obtained from PP and TG spectroscopy. The $2p_\pm$ state appears to either relax through an intermediate state or have an additional dephasing component $T_x$. We attribute the extra dephasing to two effects: (a) the thermal or optical coupling of the excited state to neighboring higher excited states due to the smaller binding

TABLE II. Relaxation times obtained from steady-state and time-resolved techniques for the $2p_0$ and $2p_\pm$ excited states in Si:Mg. From left to right: Infrared, pump-probe, transient grating, and photon echo spectroscopy.

| Excited state | $\hbar/\gamma$ (ps) | $T_1$ (ps) | $2T_G$ (ps) | $2T_E$ (ps) |
|---|---|---|---|---|
| $2p_0$ | 5.5 | 9 | 12 | 10 |
| $2p_\pm$ | 13 | 30 | 30 | 14 |

energy compared with the $2p_0$ state and (b) the interaction with nonequilibrium phonons. Extra dephasing could happen when the nonvanishing lattice (two-phonon) absorption excites nonequilibrium phonons in Si. A further investigation with improved temperature control, e.g., mounting the sample in an exchange gas cryostat, could help to answer this question. However, dominant relaxation channels cannot be unveiled with the methods used here. Understanding relaxation pathways through specific intermediate states requires advanced techniques such as time-resolved two-color detection schemes (e.g., the combination of two FELs), which are currently not available.

## V. CONCLUSION

We have used complementary time-resolved techniques to revisit intracenter relaxation dynamics of Mg, a neutral double donor center, in Si. We performed experiments at two different infrared free-electron laser (FEL) facilities, ELBE and HFML-FELIX. The well-established degenerate pump-probe method reveals a short and a long characteristic recovery time of the optical transmission. Additionally, the coherent artifact and another, yet unknown negative signal component appear, which might be related to a light-induced

shift in the resonance frequencies, e.g., by the optical Stark effect.

To assign the different decay processes, we utilized photon echo (PE) and transient grating (TG) spectroscopy. Both techniques support the short PP recovery times being identified as the excitation lifetime $T_1$ (see Table II). The TG method proves to be an excellent supplementary technique to investigate lifetimes of excited impurity states in semiconductors.

The fast PE response of the $2p_\pm$ state may confirm a multistep relaxation pathway or is caused by an additional dephasing component $T_x$.

The derived lifetimes of $(10 \pm 1)$ ps and $(30 \pm 3)$ ps for the $2p_0$ and $2p_\pm$ states, respectively, indicate ultrafast relaxation, much faster than previously reported for all single-electron donors in Si. An exception is Bi, where the $2p_0$ state is resonantly and the $2p_\pm$ nearly resonantly coupled to the $1s(A_1)$ ground state by the TO phonon ($E_{TO} = 57.5$ meV) [7].

A possible enhancement of the two-step phonon-assisted relaxation process in Si:Mg could be due to a resonant coupling of an optical phonon with the $1s(E)$ or $1s(T_2)$ intermediate states to the $1s(A_1)$ state [12,26].

[1] N. Q. Vinh, P. T. Greenland, K. Litvinenko, B. Redlich, A. F. G. van der Meer, S. A. Lynch, M. Warner, A. M. Stoneham, G. Aeppli, D. J. Paul, C. R. Pidgeon, and B. N. Murdin, Silicon as a model ion trap: Time domain measurements of donor Rydberg states, Proc. Natl. Acad. Sci. USA **105**, 10649 (2008).

[2] P. T. Greenland, S. A. Lynch, A. F. G. van der Meer, B. N. Murdin, C. R. Pidgeon, B. Redlich, N. Q. Vinh, and G. Aeppli, Coherent control of Rydberg states in silicon, Nature (London) **465**, 1057 (2010).

[3] N. Deßmann, S. G. Pavlov, V. N. Shastin, R. K. Zhukavin, V. V. Tsyplenkov, S. Winnerl, M. Mittendorff, N. V. Abrosimov, H. Riemann, and H.-W. Hübers, Time-resolved electronic capture in $n$-type germanium doped with antimony, Phys. Rev. B **89**, 035205 (2014).

[4] J. C. McCallum, B. C. Johnson, and T. Botzem, Donor-based qubits for quantum computing in silicon, Appl. Phys. Rev. **8**, 031314 (2021).

[5] H.-W. Hübers, S. G. Pavlov, S. A. Lynch, T. Greenland, K. L. Litvinenko, B. Murdin, B. Redlich, A. F. G. van der Meer, H. Riemann, N. V. Abrosimov, P. Becker, H. J. Pohl, R. K. Zhukavin, and V. N. Shastin, Isotope effect on the lifetime of the $2p_0$ state in phosphorus-doped silicon, Phys. Rev. B **88**, 035201 (2013).

[6] M. Steger, A. Yang, D. Karaiskaj, M. L. W. Thewalt, E. E. Haller, J. W. Ager, M. Cardona, H. Riemann, N. V. Abrosimov, A. V. Gusev, A. D. Bulanov, A. K. Kaliteevskii, O. N. Godisov, P. Becker, and H.-J. Pohl, Shallow impurity absorption spectroscopy in isotopically enriched silicon, Phys. Rev. B **79**, 205210 (2009).

[7] N. Stavrias, K. Saeedi, B. Redlich, P. T. Greenland, H. Riemann, N. V. Abrosimov, M. L. W. Thewalt, C. R. Pidgeon, and B. N. Murdin, Competition between homogeneous and inhomogeneous broadening of orbital transitions in Si:Bi, Phys. Rev. B **96**, 155204 (2017).

[8] M. Wienold, S. G. Pavlov, N. V. Abrosimov, and H.-W. Hübers, High-resolution, background-free spectroscopy of shallow-impurity transitions in semiconductors with a terahertz photomixer source, Appl. Phys. Lett. **114**, 092103 (2019).

[9] N. Sclar, Survey of dopants in silicon for 2–2.7 and 3–5 $\mu$m infrared detector application, Infrared Phys. **17**, 71 (1977).

[10] S. G. Pavlov, N. Dessmann, A. Pohl, V. B. Shuman, L. M. Portsel, A. N. Lodygin, Yu. A. Astrov, S. Winnerl, H. Schneider, N. Stavrias, A. F. G. van der Meer, V. V. Tsyplenkov, K. A. Kovalevsky, R. K. Zhukavin, V. N. Shastin, N. V.

Abrosimov, and H.-W. Hübers, Dynamics of nonequilibrium electrons on neutral center states of interstitial magnesium donors in silicon, Phys. Rev. B **94**, 075208 (2016).

[11] R. J. S. Abraham, A. DeAbreu, K. J. Morse, V. B. Shuman, L. M. Portsel, A. N. Lodygin, Yu. A. Astrov, N. V. Abrosimov, S. G. Pavlov, H.-W. Hübers, S. Simmons, and M. L. W. Thewalt, Further investigations of the deep double donor magnesium in silicon, Phys. Rev. B **98**, 045202 (2018).

[12] S. G. Pavlov, S. A. Tarelkin, V. S. Bormashov, N. Stavrias, K. Saeedi, A. F. G. van der Meer, N. A. Bekin, R. K. Zhukavin, V. Shastin, M. S. Kuznetsov, S. A. Terentiev, S. A. Nosukhin, D. D. Prikhodko, V. D. Blank, M. Wienold, and H.-W. Hübers, Dynamics of infrared excitations in boron doped diamond, Diamond Relat. Mater. **92**, 259 (2019).

[13] D. D. Prikhodko, S. G. Pavlov, S. A. Tarelkin, V. S. Bormashov, S. G. Buga, M. S. Kuznetsov, S. A. Terentiev, S. A. Nosukhin, H.-W. Hübers, and V. D. Blank, Intracenter dipole transitions of a hydrogen-like boron acceptor in diamond: Oscillator strengths and line broadening, Diamond Relat. Mater. **120**, 108629 (2021).

[14] N. A. Bekin, Multiphonon relaxation of the $1s(T_2)$ states of a singly ionized selenium donor in silicon, Semiconductors **54**, 1112 (2020).

[15] Yu. A. Astrov, V. B. Shuman, L. M. Portsel, A. N. Lodygin, S. G. Pavlov, N. V. Abrosimov, V. N. Shastin, and H.-W. Hübers, Diffusion doping of silicon with magnesium, Phys. Status Solidi A **214**, 1700192 (2017).

[16] V. B. Shuman, Yu. A. Astrov, A. N. Lodygin, and L. M. Portsel, High-temperature diffusion of magnesium in dislocation-free silicon, Semiconductors **51**, 1031 (2017).

[17] V. B. Shuman, A. A. Lavrent'ev, Yu. A. Astrov, A. N. Lodygin, and L. M. Portsel, Diffusion of interstitial magnesium in dislocation-free silicon, Semiconductors **51**, 1 (2017).

[18] L. M. Portsel, V. B. Shuman, A. A. Lavrent'v, A. N. Lodygin, N. V. Abrosimov, and Yu. A. Astrov, Investigation

of the magnesium impurity in silicon, Semiconductors **54**, 393 (2020).

[19] S. G. Pavlov, Yu. A. Astrov, L. M. Portsel, V. B. Shuman, A. N. Lodygin, N. V. Abrosimov, and H.-W. Hübers, Magnesium-related shallow donor centers in silicon, Mater. Sci. Semicond. Process. **130**, 105833 (2021).

[20] S. G. Pavlov, L. M. Portsel, V. B. Shuman, A. N. Lodygin, Yu. A. Astrov, N. V. Abrosimov, S. A. Lynch, V. V. Tsyplenkov, and H.-W. Hübers, Infrared absorption cross sections, and oscillator strengths of interstitial and substitutional double donors in silicon, Phys. Rev. Mater. **5**, 114607 (2021).

[21] B. Pajot, in *Optical Absorption of Impurities and Defects in Semiconducting Crystals*, edited by M. Cardona, P. Fulde, K. von Klitzing, R. Merlin, H.-J. Queisser, and H. Störmer, Springer Series in Solid-State Sciences Vol. 158 (Springer, Berlin, 2010).

[22] S. L. Palfrey and T. F. Heinz, Coherent interactions in pump–probe absorption measurements: The effect of phase gratings, J. Opt. Soc. Am. B **2**, 674 (1985).

[23] K. Litvinenko, N. H. Le, B. Redlich, C. R. Pidgeon, N. V. Abrosimov, Y. Andreev, Z. Huang, and B. N. Murdin, The multi-photon induced Fano effect, Nat. Commun. **12**, 454 (2021).

[24] J. A. Shields, M. E. Msall, M. S. Carroll, and J. P. Wolfe, Propagation of optically generated acoustic phonons in Si, Phys. Rev. B **47**, 12510 (1993).

[25] F.-W. Deeg, Transient grating spectroscopy, in *Dynamics during Spectroscopic Transitions* (Springer, Berlin, 1995), pp. 456–505.

[26] V. N. Shastin, R. K. Zhukavin, K. A. Kovalevsky, V. V. Tsyplenkov, V. V. Rumyantsev, D. V. Shengurov, S. G. Pavlov, V. B. Shuman, L. M. Portsel, A. N. Lodygin, Yu. A. Astrov, N. V. Abrosimov, J. M. Klopf, and H.-W. Hübers, Chemical shift and exchange interaction energy of the $1s$ states of magnesium donors in silicon. The possibility of stimulated emission, Semiconductors **53**, 1234 (2019).